Aerosols and carbonaceous and nitrogenous compounds emitted during the combustion of dead shrubs according to twigs' diameter and combustion phases

T. Barboni, L. Leonelli, P.-A. Santoni, V. Tihay-Felicelli

Aerosols and carbonaceous and nitrogenous compounds emitted during the combustion of dead shrubs according to twigs' diameter and combustion phases

T. Barboni, L. Leonelli, P.A. Santoni, V. Tihay-Felicelli

University of Corsica – CNRS UMR 6134 SPE, Campus Grimaldi, BP 52, 20250 Corte, France

Corresponding author:

Toussaint Barboni

University of Corsica – CNRS UMR 6134 SPE, Campus Grimaldi, BP 52, 20250 Corte, France,

Phone: +33 495 450 046, Fax: +33 495 450 162, E-mail address: barboni@univ-corse.fr

Abstract:

Smoke from forest fires is hazardous to health and can result in losses of respiratory function and vision. The knowledge of the chemical constituents in such smoke is an important objective. In this study, leaves and branches and twigs of *Cistus Monspeliensis* were burned with a cone calorimeter and the emitted smoke was analysed by non-dispersive infrared (NDIR) spectroscopy, He-Ne laser method, Fourier-transform infrared (FTIR) spectroscopy, and automated thermal-desorption–gas-chromatography/mass-spectrometry (ATD-GC/MS). These techniques were used during various combustion phases: prior to ignition and during flaming and glowing phases. The influence of branch diameter on chemical composition was examined. Analysis of the smoke reveals the presence of CO_2, H_2O, CO, aerosols, CH_4, NO, and other gases in smaller proportions, as well as non-methane organic compounds (NMOCs). 96% of the carbon present in the fuel was found in the emitted smoke. CO_2 is the gas mainly emitted and its level is independent of the diameter of the cistus branch burned. It is mainly emitted in the flaming phase, unlike CO, which is emitted during the glowing phase. Aerosols are emitted principally during the pre-ignition stage. The mass loss is higher during the flaming phase than during the glowing one because the burning occurs under well-ventilated condition. During the glowing phase, the mass loss is only due to the char oxidation. The calculation of the modified combustion efficiency confirms those operating conditions.

Keywords: smoke emission, emission factor, gases, VOC, combustion phases, aerosols

Nomenclature

a	Aerosol
b	Burned
EF	Emission factor ($g.kg^{-1}$)
CMB	Carbon mass balance ($g_C.kg^{-1}$)
dry	Dry
EC	Elemental Carbon (µg)
FC	Fuel consumption (-)
FID	Flame ionization detector
FMC	Fuel moisture content on dry basis (%)
FTIR	Fourier transform infrared
k	Light extinction coefficient (m^{-1})
m	Mass (kg)
m_a	Aerosols mass (kg)
MCE	Modified combustion efficiency (-)
n_c	Number of carbon atoms (-)
NMOC	Non-methane organic compounds
NDIR	Non-dispersive infrared
OC	Organic carbon (µg)
O_2	Oxygen
t	Time (s)
T	Temperature (K)
$\dot{V}$	Standard flow rate in the exhaust duct at 298 K ($m^3.s^{-1}$)
VOC	Volatile organic compound
w	Molecular weight ($kg.mol^{-1}$)
σ_a	Specific extinction area ($m^2.kg^{-1}$)

1. Introduction

Forest fires are major problems, in 2007, nearly 350 million hectares burned globally including 700,000 hectares in Europe [1]. France, with 15 million hectares of forest, is a country that is particularly vulnerable to forest fires, as are other Mediterranean regions. On average, 2,077 forest fires were recorded each year in France over past 20 years, which represents an average annual burnt surface area of 12,000 ha [2]. These fires can be of natural or anthropogenic origin. They cause human tragedy, significant economic losses, and damage the ecosystem. Global warming may also increase the frequency and consequences of fires. Beyond their destructive aspects, forest fires also emit large quantities of smoke. Consequently, these fires present risks to exposed individuals because this smoke is toxic and opaque. Smoke opacity leads to decreased vision [3], which impacts the work of fire-fighting staff and the orientation of victims. Smoke also affects the overall composition of the atmosphere. In recent years, fires have led to serious health problems and multiple deaths as a result of air pollution in Indonesia, Malaysia, Central America, Russia, Mexico, and the United States [4]. Langmann et al., [5] estimated that about 40% of the CO, 35% of the carbon particles, and 20% of the total nitrogen oxides (NOx) emitted into the atmosphere are the result of biomass combustion. Forest fires also produce high levels of fine ($PM_{2.5}$) and ultrafine (PM_1) particles [6]. In particular, $PM_{2.5}$ is believed to be responsible for 0.8 million premature deaths around the world, according to Cohen et al., [7]. In addition, according to the WHO [8], at least 1.4% of all deaths worldwide are caused by air pollutants, which are also factors that decrease life expectancy (by 8.2 months in Europe). However, there has been a recent increase in awareness of the health risks posed by smoke inhalation from wildfires. This report highlights several elements related to the gradual loss of respiratory function over multiple seasons, and the deterioration in the general health of fire fighters. The conclusions made were considered sufficiently disturbing by the Ministry of the Interior (French Ministry) to commission a health survey by IGAS (General Inspectorate of Social Affairs). A previous report on the mortality of professional fire fighters in France by the same organization [9] concluded that overall cancer mortality is not statistically different from that of the general population. But, the study observed that there was a moderate but not significant increase for some cancers.

Smoke emitted during forest fires is composed of gases and suspended solid residues, liquid particles ashes coming from incomplete combustion. Smoke contains a complex mixture of gases, volatile organic compounds (VOCs) and aerosols [10-14].

These primary pollutants undergo physicochemical transformations in the atmosphere that give rise to secondary pollutants. CO_2 and CO are the most abundant compounds emitted by wildfires. They represent between 90 and 95% of the total amount of carbon emitted in smoke [15]. The gases emitted are function of the plant species that burns, the ventilation regime and the ratio between the flaming and smoldering combustion phases. Some gases are emitted only during the flame phase and others are emitted during the glowing phase. These characteristics can be integrated into emission models. VOCs and in smaller proportions semi-volatile organic compounds (SVOCs), which include aliphatic hydrocarbons (such as propane), aromatic hydrocarbons (such as benzene), phenol derivatives (such as cresols), oxygenated compounds (such as alcohols), aldehydes (such as formaldehyde and acrolein), ketones, carboxylic acids are formed [14]. PAHs (polycyclic aromatic hydrocarbons), furans, and esters are also emitted [14]. Among identified VOCs, aliphatic hydrocarbons and oxygenates as well as benzene family are the most abundant. Their proportion varies according to the fuel and the type of forest and the method for trapped these compounds [15-22]. Suspended particulate matter (PM) represent 5% of the emitted carbon [23]. PM are of major interest, both in terms of health and environmental impact. PM are a complex mixture of organic and inorganic substances. These particles are composed of elemental carbon (EC), organic carbon (OC) and ions [24]. Elemental carbon, also referred to as black carbon (BC) or soot, is a primary compound produced by the incomplete combustion of carbonaceous fuels.

Many studies analysed the composition of smoke emitted by wildfires under fire conditions during prescribed burns or in the laboratory. Outdoor studies (forest fires and prescribed burns) have been conducted on different types of vegetation around the world, including savannahs and African grasslands [25-26], the Brazilian Amazon rainforest [27], Canadian boreal forests [18], North American coniferous forests [28-29], the temperate ecosystems of Greece [12] and the maquis and forests of Mediterranean ecosystems [14, 30-31] and Australia [32]. Akagi et al., [19] and Andreae and Merlet [15] studied emissions from all types of worldwide wildfire (savannahs, grasslands, tropical and extratropical forests, maquis, crop residues, and peat) in order to provide usable emissions data for input data in atmospheric models. Urbanski et al., [33] published data of pollutants from prescribed burning in forests (temperate, boreal, and tropical), scrubland and savannah, while Yokelson et al., [34] reported emission data from several types of wildfire in Mexico. Pio et al., [35] showed that, due to the combustion process, emissions depend on the type of burned forest as well as the weather conditions. Laboratory studies have also been carried out on the smoke produced by the combustion of vegetation [36-37].

Although laboratory-scale experimental conditions are quite different to those of a field-scale fire, these studies can refine results for species and let testing analytical techniques. This scale allows to better identify the compounds in smoke and provide a more detailed understanding of the reaction mechanisms involved in the formation of these compounds. Soares Neto et al., [36] studied emissions from the combustion of 12 representative plants of the Amazonian ecosystem using a ~16 m^3 combustion chamber and obtained results that agreed with emissions measured in the field during fires in the Brazilian Amazon rainforest [27].

The aim of the emission models is to assess the pollutants emitted in order to predict their potential effects on the health of humans or the atmospheric pollution. The current approaches used in the literature in order to predict atmospheric emissions from forest fires, from the point of view of the safety of firefighters and population, are based on semi-physical and empirical fire spread models (mainly Rothermel's model) coupled with atmospheric models like WRF, MESO-NH, etc. Such model of fire spread use one equation (a thermal balance) to represent the complexity of forest fire. No equation is used in these models neither to represent the degradation (pyrolysis) of the vegetation nor to represent the gaseous combustion of those degradation gases and ensuing smoke, nor the smouldering combustion of the remaining char. Thus, these models only produce global emissions and cannot take into account the variation of emission during the different emission phases or due to the vegetation size [38]. This is a major lack for modelling since for instance, the preheating of the vegetation located ahead of a fire front will depend on the size of the particles. The finest particles will be heated more rapidly that the coarsest and they will mainly contribute to the emission. Conversely, once the active fire front has leaved the area of interest, the remaining large particles will continue to burn (more or less actively as function of the wind) and their emission during the flaming phase will be different from that observed after the flameout. One way to take into account these phenomena is the use of physical models. These last ten years, different approaches have been developed such as WFDS [39] or Firestar [40]. These models can represent the finest physical phenomenon involved in combustion: heat and mass transfer modelling, flow and gaseous combustion modelling, degradation of the solid fuel (the vegetation) with the possibility to use emission factors, turbulence, etc. Such models consider the vegetation as a porous medium made of different classes of particles. These particles classes are based on the state of the vegetation (dead or alive) and also on their characteristics thickness. For instance, a class is defined for the alive leaves, another for the dead.

In order to take into account precisely the contribution of vegetation, it is therefore necessary to develop fire behaviour fuel models able to represent the different classes of particles. This

point constitutes a challenge given the diversity of vegetation that may be subject to forest fires. Such work has begun in different European project (Fire Star 2002-2005, EuFirelab 2002-2006) for the vegetation of some countries (France, Spain, Portugal, Greece, etc.). Thus there exist databases for some wildland fuels in Europe that allows to consider the complexity of actual fuel. However, those databases must be completed in order to take into account as many vegetative fuels as possible. Currently we have provided such data for *Cistus Monspeliensis* [41]. With these fire behaviour model and by using physical fire spread models (like WFDS) a possibility exist to predict the fire emission at the fuel particle level by considering not only the different phases of the burning (preheating, flaming combustion, smouldering) but also the size of the particles involved in the burning. Hence, the combination of a physical model of fire spread that allows to represent the different stages of combustion (taking intrinsically into account the wind and topography) and a fire behaviour fuel model adapted to the vegetation plant of interest (description of the different classes of particles) will be in a near future a powerful tool for the prediction of wildfire emissions. Then the transport in the atmosphere will need the coupling with an atmospheric model.

The present work aims to characterise the pollutants emissions produced by the burning of a plant species of the Mediterranean maquis with a cone calorimeter. Cistus Monspeliensis represents nearly 20,000 ha of surface in Corsica. After a fire, there is a massive growth of Cistus because these plants are pyrophilic species. Cistus Monspeliensis was cut according to plant-fragment size (leaves and 1–20 mm diameter twigs) and the compounds emitted were identified and quantified as function of the size of the burned particles and combustion phases (pre-ignition, flaming, and glowing). This study provides refined data on emission factors that can be used as input data in coupled atmosphere-fire spread models according to the combustion phases that occur in the different fire areas. Ahead of the fire front the pollutant are emitted because of the preheating. In the flame front the pollutants emissions are due to the burning of the fine vegetation (leaves and twigs with diameter lower than 4 mm are engulfed in flames; Tihay-Felicelli et al., [42]. Behind the flame front (glowing phase), the pollutants emission is caused by the largest branches and embers that continue to burn. The first section of this paper presents the fuel as well as the material and method used to characterize the compounds emitted during the degradation and combustion of the forest fuel and the calculation of the emission factors. The second section is devoted to the presentation of the results and the corresponding discussions.

In this section, the mass loss during the preheating and the burning of vegetation leaves and twigs are first presented as well as the heat release rate and the smoke production rate in order to understand the different phases involved (preheating, flaming, glowing). Then, the pollutants emitted are characterized (identification and quantification), on one hand according to the thickness of the forest fuel and on the other hand according to the phase of emission. The emission factors corresponding to those pollutants are provided. Finally, a carbon balance was done in order to assess the quality of our analyses.

2. Materials and methods

2.1. Fuel sample

Experiments were performed with leaves, branches and twigs of *Cistus Monspeliensis*. The materials used in this study were collected in central Corsica from live shrubs. In order to remove the moisture of the samples, the fuel was oven dried at 60°C during 48 h. Ultimate analysis data values are listed in Table 1.

Table 1. Ultimate analysis data, and higher and lower heating values for *Cistus Monspeliensis*

	C (%)	H (%)	O (%)	N (%)
Leaves	48.5	5.9	44.3	0.6
Twigs	49.3	5.5	44.8	0.3

Leaves (average thickness of ~0.75 mm) were collected and placed in a 100 cm² ventilated basket. The sample holder was filled such that leaf superposition was avoided. Twigs with diameters between 1 and 20 mm were selected and cut to 10 cm lengths before being placed in the same basket (Fig. 1). Twig diameters were determined using a Mitutoyo® Quick Micrometer (precision: 0.01 mm). To ensure that the fuel surfaces undergo the same heat flow from the cone heater, the same apparent fuel surface was maintained for all diameters. The calculated area of the twigs corresponds to the surface of the twigs which are subjected to the thermal flux of the calorimetric cone. Before each experiment, a photo of the sample holder with the fuel inside was taken in order to check its apparent surface using image processing with Matlab® software. Next, image processing was used to determine the apparent surface area of the fuel, which was 80 cm² (this corresponds to the area of a basket full of 1 mm twigs)

with a standard deviation of 6 cm^2. This approach allows us to study the effect of each size of vegetation for the emission of smoke. Predicting wildfire emissions require understanding the emission as function of the diameter vegetation i.e. size of twigs or branches level.

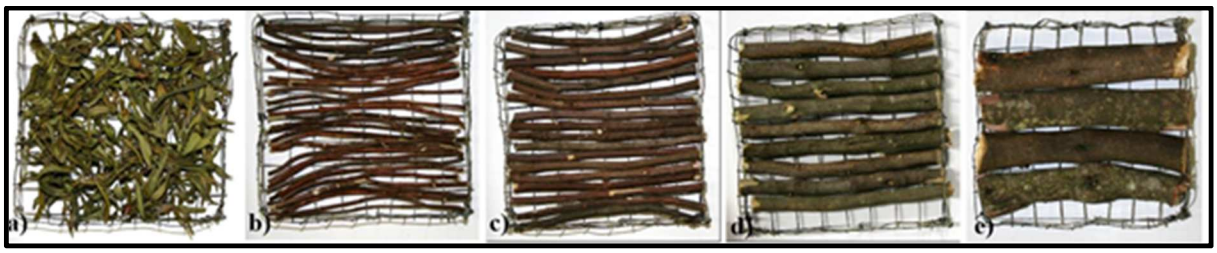

Figure 1. Sample holder containing cistus samples of various characteristic thicknesses: (a) leaves, (b) 2 mm, (c) 4 mm, (d) 8 mm, and e) 15 mm diameter twigs.

2.2. Experimental methods

Fuel samples were burned using a cone calorimeter (Fig. 2) coupled to an Antaris IGS FTIR Spectrometer (ThermoFisher Scientific). The cone calorimeter is composed of a cone heater, a shutter, a load cell, and an exhaust system with gas analyzers. Samples were exposed to a radiant heat flux of 50 $kW.m^{-2}$. This value was chosen because it corresponds to the levels of heat flux measured in shrubland fires ahead of a fire front [43]. The fuel is preheated by the cone heater which leads to its gasification. An ignition occurs after a time delay that depends on the size of the samples. The time of ignition was determined using high-speed camera movies to clearly determine the onset of the flaming stage. Then the sample burning occurred in two stages. Flaming combustion is observed first. Its duration depends on the thickness of the sample and available mass. Then, once the flames extinguish, only the embers remain. Glowing combustion follows. By using an open basket, the combustion is over ventilated and all the fuel burns. After the complete consumption of embers, the extinction occurs and only ashes remain. Further cone calorimeter details are provided in a previous publication [38].

The heat release rate is given by the oxygen molar flow rate:

$$\mathrm{HRR} = E\left(\dot{n}_{O_2}^{0} - \dot{n}_{O_2}\right)W_{O_2} \quad (1)$$

where E is equal to 13.93 MJ.kg^{-1} for cistus and corresponds to the heat release per unit mass of O_2 consumed, $\dot{n}_{O_2}^0$ and $\dot{n}_{O_2}$ represent respectively the molar flow rates of O_2 in the incoming air and in the exhaust duct and W_{O_2} is the molecular weight of oxygen. More details on HRR measurement are given in a previous study [38].

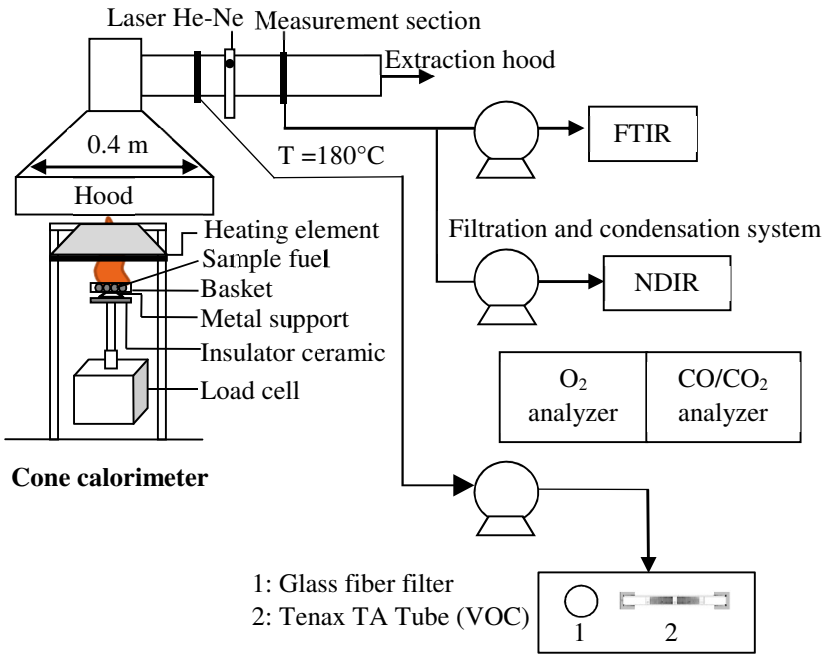

Figure 2. Experimental device: schematic of the cone calorimeter and analysers for determining the sampled gas, VOCs, and aerosols

2.3. Chemical analysis of smoke and emission factors

Smoke from forest fires includes important amounts of gases, aerosols (PM) and other chemical compounds like volatile organic compounds (VOCs). The generation of combustion products was quantified in terms of emission factors, EF_i (g.kg^{-1}), defined as the mass of chemical species i produced per dry mass of fuel burned, $m_{b,dry}$ [15].

$$EF_i = \frac{m_i}{m_{b,dry}} \quad (2)$$

where m_i (kg) is the mass of compound i released by the burning and $m_{b,dry}$ (kg) is the dry mass burned during the experiments.

The exhaust gases of combustion were sampled from the exhaust ducts of the cone calorimeter (see Fig. 2) and passed through four different analyzers. The first measurement system consists of an Antaris Industrial Gas System (IGS) FTIR-based analyzer from ThermoFisher Scientific. The FTIR spectrometer allowed to obtained the molar fractions of CO_2, CO, CH_4, NO, NO_2, NH_3, C_2H_6, C_2H_4, C_2H_2, C_3H_8, C_3H_6, C_4H_6, C_6H_6, HCHO, CH_3CHO, SO_2, H_2O (and also CO_2, CO in addition to NDIR). A filter removing the aerosols was placed before the gas cell and the sampling line was heated at 180°C to avoid condensation. The spectrometer was equipped with a MCT-A detector and a gas cell measurement of volume 0.2 L with an optical path-length of 2 m. IR spectra were recorded in the spectral range of 4500-550 cm^{-1} with a 0.5 cm^{-1} resolution. The flow rate of the sampling pump was adjusted to 3.5 $L.min^{-1}$. The identification of the compounds by FTIR was carried out from a bank in which the products resulting from the combustion are listed. Calibration verification is performed once a year by a maintenance engineer from Thermofisher. The second measurement system consists of non-dispersive infrared (NDIR) spectroscopy. This apparatus was used to quantify continuously CO and CO_2. Each day of analysis, NDIR analysers were calibrated with two points of measurement. The first point corresponds to a gas without CO and CO_2. For this, almost pure N_2 (99.995% i.e. 4.5) was used. For the second point, a mixture containing 2500 ppm of CO and 8% for CO_2 was used. Finally, a double check was made with the CO and CO_2 data recorded with the FTIR. The third analyzer corresponds to a He-Ne-laser for the measurement of aerosols. Finally, the fourth analyzer consists of a ATD/GC/MS for VOCs identification and quantification. A sample pump with a flow rate of 2 $L.min^{-1}$ (see Fig. 2) was used to collect VOCs with Tenax tubes (Supelco®, Saint-Quentin Fallavier, France). Upstream of the pump a filter was used to prevent the aerosols penetrate the Tenax TA tube. Since the sampling takes place in the smoke extraction pipe where the flow rate is 24 $L.s^{-1}$ a multiplicative factor of 720 was used to calculate the emission factors. During the experiment, a collecting system of 3 tubes connected in parallel to a three-way valve was used in order to sample the smoke as a function of the different phases, namely the pre-ignition, flaming and glowing phases. A least three tests were carried out to ensure the reproducibility for the leaves and for each size of fuel twigs (1 to 20 mm). The Tenax TA sorbent tubes used for the analyses have the following dimensions 11.5 cm × 6 mm outer diameter (o.d.) × 4 mm inner diameter (i.d.), in order to capture the organic compounds (C_5-C_{30}). The analyses were performed by thermal desorption using an automatic thermal desorption–gas chromatography–mass spectrometry apparatus (ATD-GC/MS). It should be noted that sorbent tubes have previously been used in other studies for sampling VOCs and SVOCs [44-45] before GC/MS analysis.

The analyses were carried out immediately after filling the Tenax tubes using an ATD TurboMatrix from PerkinElmer. For the thermal desorption of VOCs, H_2 flow was set at 30 $mL.min^{-1}$ with a column head pressure at 25 psi. The sorbent tube was brought to 280°C over 10 min and a carrier gas flushed the sample towards a cold trap at 5°C.

In a second step, the cold trap (22 cm, 0.53mm i.d.; Supelco) was programmed to increase temperature from 5° to 280°C at $40°C.s^{-1}$, then held isothermally at 280°C for 3 min. The compounds were then desorbed onto the chromatograph under H_2 as carrier gas via a heated transfer line maintained at 280°C. The injector temperature was set to 280°C. The ionization energy for mass detection was set to 70 eV and electron ionisation mass spectra were acquired over the mass range 35–350 Da. The chromatograph and the mass spectrometer were Perkin Elmer Clarus 500® apparatus (Waltham, MA, USA). The chromatograph was equipped with a non-polar column (Rtx®-1 fused silica column, dimethylsiloxane, Resteck, Lisses, France), length 60 m and i.d. 0.22 mm. This column was coupled with the mass detector. Detection was carried out by a quadripolar analyzer made up of an assembly of four parallel electrodes of cylindrical section. The oven temperature of the chromatograph was programmed from 50° to 260° C at $2°C\ min^{-1}$ and then held isothermally at 260°C for 10 min. The methodology used to identify individual components was based on i) the comparison of their GC retention indices (RI) on non-polar columns with those of authentic compounds or literature data [45-46]. The RIs on nonpolar columns were determined relative to the retention time of a series of n-alkanes with linear interpolation. The results were computer-matched with commercial mass spectrum libraries [46] and spectra were compared with those in our own library of authentic compounds. The majority of these compounds were commercial standard components. The relative amounts of the individual components were calculated on the basis of their GC peak areas, obtained on a second capillary Rtx-1 column, without flame ionisation detector (FID) response factor correction.

Quantification was performed for equivalent benzene with GC/FID. The method of external calibration was used from a commercial standard (Restek, Lisses, France). Triplicate injections of standards were made for each set of concentrations (5 different concentration) for the curves of external calibration standards. A total of 15 calibration points were made. The correlation coefficient (R^2) for the linear regression of the curve of external calibration standards is 0.996, indicating a good correlation between the detector's response and the concentration of injected products. The identification and quantification methods of the chemical compounds were described in a previous study [48].

Before each sampling, Tenax tubes are conditioned for 15 minutes at 280 ° C. Each day, a "blank analysis" is performed after conditioning the tubes to avoid or observe contaminants.

Smoke obscuration was measured in the exhaust duct with a He-Ne laser (0.5 mW nominal power) emitting at the red wavelength of 632.8 nm. The length of the optical path in the exhaust duct is 11.4 cm. The smoke production rate (SPR) was calculated according to the basic smoke equation:

$$SPR = k\dot{V} \quad (3)$$

where k is the light extinction coefficient given by the Bouguer's law and $\dot{V}$ is the standard flow rate in the exhaust duct. Aerosols were collected on glass fiber filters (37 mm diameter) sampled in the cone calorimeter duct by using a sample pump (see Fig. 2). The mass of aerosol (m_a) released during the burnings was calculated with the following equation:

$$m_a = \int_0^T \frac{k}{\sigma_a} \dot{V}\, dt \quad (4)$$

where σ_a (m^2/kg) is the specific extinction area. The values obtained by leonelli et al., [49] for σ_a were used: σ_a = 8290 m^2/kg during the flaming stage and σ_a = 3290 m^2/kg during the preheating and smoldering stage.

The Elemental Carbon (EC) and Organic Carbon (OC) analyses of the aerosols were done with a technique that combines evolutionary thermal optical analysis (TOA) and flame ionisation detection (FID) by the Analytice® company, according to the NIOSH 5040 method. The measurement of EC and OC contents as well as their ratio is a first step in the realization of a mass balance carbon, essential for a better knowledge of the sources particles. EC refers to soot carbon, a purely primary compound, related to pure graphite. It is emitted during combustion processes. OC comes either from thermal degradation or organic compounds from the smoke that adsorbs on the particles already formed during combustion

A total carbon mass balance (CMB) was used to check the quantities of emitted gases. Indeed, when quantifying emitted compounds, one must check that the analysed carbon content does not exceed that found in the plant by ultimate analysis. Hence, the amount of carbon CMB_i of each assayed compound i, was calculated in grams of carbon per kilogram of plant according to the equation:

$$CMB_i = EF_i \times \frac{W_c}{W_i} \times n_c \quad (5)$$

where W_C and W_i are the molecular weights of carbon and compound *i*, respectively and n_C is the number of carbon atoms present in compound *i*.

To evaluate the combustion completeness [15], the modified combustion efficiency (MCE) was introduced, as follows:

$$MCE = \frac{[CO_2]}{[CO_2]+[CO]} \quad (6)$$

where $[CO_2]$ and $[CO]$ are the molar concentrations of emitted CO_2 and CO in the smoke. Fire-integrated excess molar mixing ratios of CO_2 and CO were used to calculate mean modified combustion efficiencies.

2.3. Statistical Analysis

A multiple-sample comparison test (STATGRAPHICS® Centurion XV) was used. We selected the ANOVA test to highlight any statistically significant difference between the values measured in all the experiments. If a probability value (p) obtained using the F test is less than 0.05, there appears a difference between the means of the variables with a confidence level of 95%. Multiple-range tests were then applied to determine which means are significantly different from each other. The method used to discriminate between the means was Fisher's least significant difference procedure.

3. Results and discussion

3.1. Mass loss, heat release rate and smoke production rate

Figure 3 displays the non-dimensional mass loss, m/m_0 (where m and m_0 are respectively the mass over time and initial mass of the samples) as functions of time for twigs samples of different thicknesses. The most characteristic thickness-size data are presented. The same behaviour was observed for all twigs diameters investigated [42]. Low mass loss is first observed prior to ignition, which corresponds to low emission of degradation gases, water vapour and aerosols and represents 4.0 ± 0.03 % loss of the initial mass for leaves and branches between 1 and 20 mm in diameter. After ignition and during the flaming phase, an increase in mass loss was observed. Fuel degradation is even more intense under the combined effects of the flame and the radiant panel.

We noted that finer thickness twigs lose mass more rapidly than thicker thickness (steeper slope in Figure 3). During the flaming stage, we observe the highest loss of mass, namely 75.0 ± 5.0 % of the initial mass. After the flameout, i.e., during the glowing phase, the mass loss represents 13.2 ± 4.0 % of the initial mass. It corresponds to the oxidation of chars. At the end of the combustion process, it remains only ashes representing 0.9 ± 0.6 % of the initial mass in the set of experiments conducted.

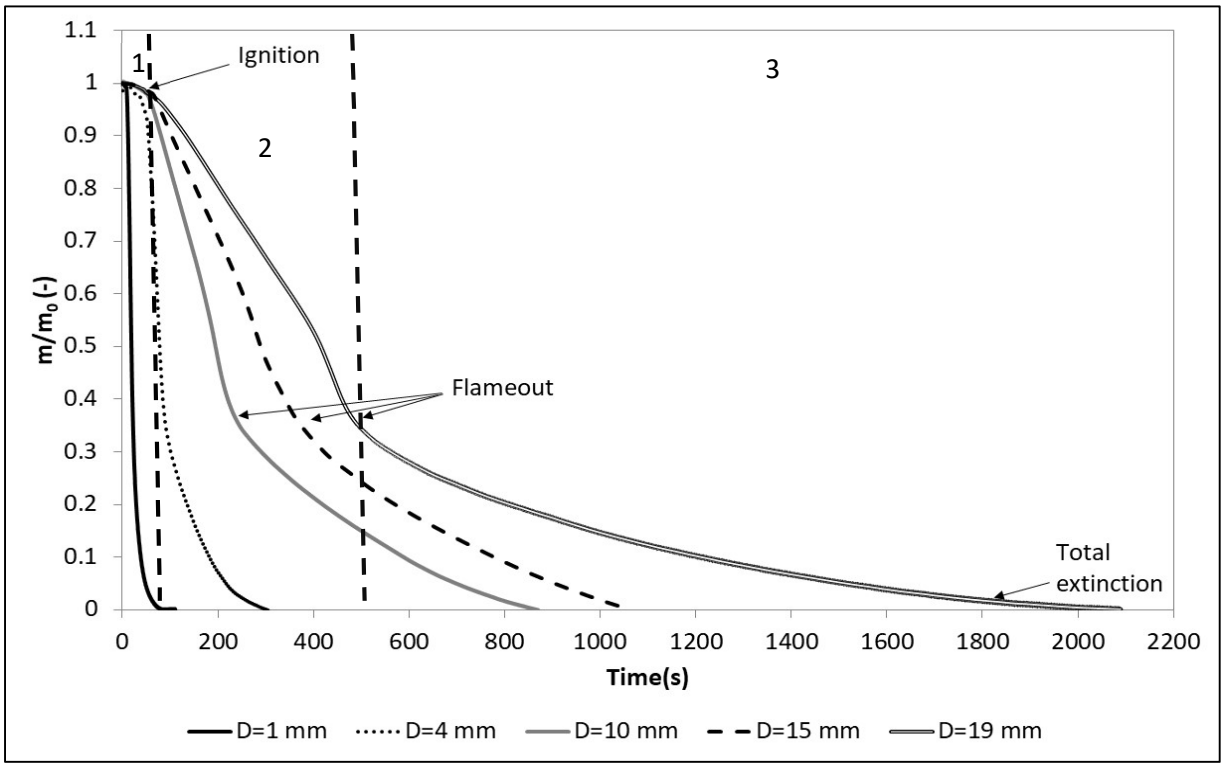

Figure 3. Non-dimensional mass loss as function of time for different characteristic thicknesses (1: pre-ignition phase, 2: flaming phase, and 3: glowing phase for 19-mm-thick branch samples). The vertical lines represent ignition and flameout times.

To understand the emissions of pollutants, it is necessary to measure the heat release rate (HRR) emitted during combustion as well as the smoke production by measuring the smoke production rate (SPR). Figure 4 shows the SPR and HRR as a function of time for the 2 and 8 mm samples. For both size of samples, the peak SPR is obtained during the ignition. According to these results, it is important to consider the preheating phase which corresponds to a significant release of smoke. The HRR increases rapidly after ignition to form a peak during the first seconds of the burning (combustion with flame). After ignition, the production of smoke is less important and two distinct behaviours can be observed according to the characteristic thickness of the samples.

For the sample with a thickness of 2 mm (thermally thin), the SPR curve forms a second peak, coinciding with the peak of HRR (Fig. 4a). Then the HRR decreases rapidly as well as the SPR until the flameout where we observe a change in slope associated with the combustion of chars. No smoke production occurs during the char combustion. For the 8 mm thick sample, two other SPR peaks are observed during the flame phase, as well as a plateau zone located between the two peaks, reflecting an almost constant smoke production. During this phase the HRR also clearly exhibits two peaks of HRR with different intensities (Fig. 4b) and a plateau corresponding to a quasi-steady flaming combustion. The second peak of HRR is higher than the first one because at this time the underside of the twigs are ignited [38]. It was not the case for the 2 mm twigs that burn as a whole. For both samples, we observe that the SPR curves are correlated with the HRR curves during the flaming stage and no SPR occurs after the flameout. For the 2 mm twigs diameter the smoke emission is mainly observed during the pre-ignition phase.

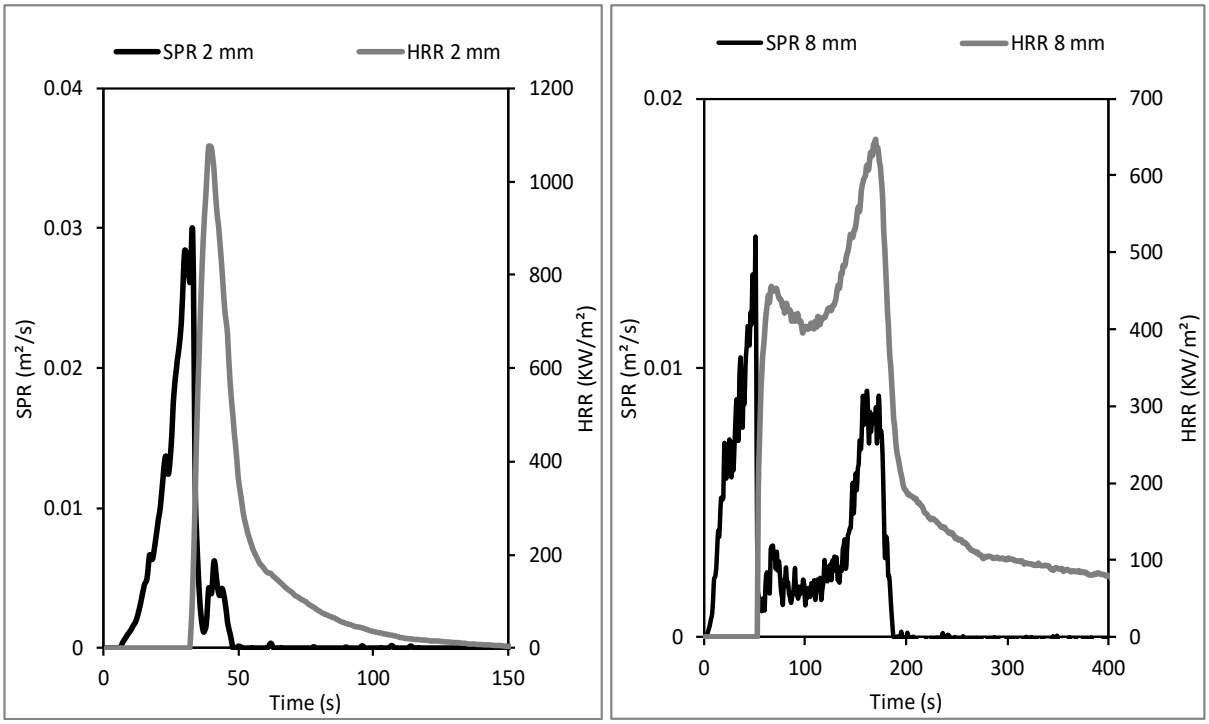

Figure 4. Mean SPR and HRR for the burning of twigs with a diameter of a) 2 mm and b) 8 mm (SPR: smoke production rate; HRR: heat release rate).

Table 2 presents the average value for the fuel mass, ash mass, ignition time, flameout time and combustion time according to the diameter of twigs and leaves. We can see that the ignition

time of the leaves (0.75 mm thick samples) is much lower than that of the thinnest twigs with a diameter of 1 mm. The mean ignition times are equal to 5.3 and 22 s for the leaves and 1 mm diameter twigs, respectively. Although the thicknesses of these two kinds of particles are very close, the leaves ignited four times faster than the smallest twigs. Concerning the twigs, a scattering is observed for the ignition time. These fluctuations were due to local changes in the temperature and species concentration of the combustible gas mixture from one experiment to another. Indeed, it should be mentioned that auto-ignition was considered in this work. We did not use neither spark ignitor nor flame ignitor. Thus the ignition depends not only on the molar fractions of the combustible gaseous and air but also on the temperature of the mixture. Since the vegetation fuel is natural, it is not made of straight sticks of wood but rather tortuous twigs. Then the radiant heater has a conical shape and although the heat flux is roughly constant at a given height under the cone, it varies from the centre of the cone (where it is maximum) to the edges (where it is minimum). A variation of 5% was measured. Hence, the heating is not the same from a sample to another since the samples are not perfectly similar and the heat flux is slightly heterogeneous, mainly on the side of the samples. Thus the degradation is spatially variable from one sample to another. The spatial variation of the degradation due to the fuel shape and the (slightly) spatial variation of the heater can lead to different ignition conditions (flammability limit and temperature) from one sample to the other. This was confirmed with observation (with a high speed camera) because the ignition point was not at the same location at the surface of the fuel for the different samples. It was however located close to the centre of the sample where the heat flux is the most homogenous. For diameters lower than or equal to 4 mm, the ignition time increases with the twig diameter. For this range of diameters, the evolution of the ignition time can be considered to be proportional to the diameter. Then for higher twigs diameter the ignition is almost constant since those samples can be consider as thermally thick.

Table 2. Averaged value for fuel and ash masses, ignition time (t_{ig}), flame out time (t_{flo}), combustion time (t_{com}) and ignition temperature (T_{ign}) according to the thickness (mm) of leaves and twigs diameter.

t (mm)	*m (g)*	*Ash (g)*	t_{ign} *(s)*	t_{flo}*(s)*	t_{com} *(min)*	T_{ign} *(°C)*
0.75	6.4±0.5	0.3±0.0	5.3±0.5	29.3±2.9	1.7±0.2	396.6±11.9
1	5.7±0.4	0.1±0.0	22.0±7.9	36.7±6.6	1.4±0.2	417.1±19.4
2	7.9±0.9	0.2±0.0	32.5±6.8	51.3±5.3	2.0±0.1	441.6±18.8
3	14.2±1.0	0.2±0.0	35.7±5.8	69.9±6.3	3.6±0.7	455.7±12.3
4	20.4±1.0	0.4±0.1	46.0±4.9	98.8±7.5	5.0±0.8	470.2±10.3
5	25.3±1.1	0.4±0.0	48.0±6.4	118.8±8.8	6.4±0.7	468.0±11.9
6	33.1±1.1	0.4±0.1	48.6±8.3	150.2±10.4	9.4±1.1	463.2±21.4
7	37.2±1.3	0.6±0.1	52.0±6.6	178.3±13.5	12.1±1.1	473.7±5.2
8	45.5±1.5	0.7±0.1	50.6±8.5	200.6±24.5	11.8±1.7	471.4±22.7
9	51.2±0.9	1.0±0.1	49.2±5.6	208.2±6.1	13.8±1.5	479.6±9.2
1	55.4±1.6	1.2±0.2	47.7±7.3	232.8±18.8	17.2±1.7	469.6±14.6
11	56.3±1.5	1.0±0.1	48.2±6.9	246.7±13.0	18.3±1.6	485.4±9.1
12	68.5±1.8	1.4±0.2	45.5±9.3	322.5±51.1	22.3±4.1	482.6±14.0
13	69.0±2.0	1.3±0.2	51.3±6.2	314.7±14.3	24.1±3.5	484.6±8.9
14	72.7±2.0	1.2±0.2	50.3±8.2	380.8±24.6	27.0±2.9	476.8±18.5
15	82.9±2.0	2.0±0.2	54.8±5.4	415.3±11.5	30.2±4.9	475.1±13.8
16	86.1±2.1	1.6±0.2	55.0±6.0	428.5±39.5	34.6±4.6	474.3±13.0
17	83.7±2.3	2.0±0.2	55.0±7.0	422.0±22.1	36.7±4.8	482.0±6.9
18	83.8±2.5	1.2±0.1	50.7±8.3	407.3±80.2	38.6±5.2	483.3±17.2
19	118.7±2.9	1.0±0.1	55.0±8.0	580.5±60.1	38.1±10.2	475.0±26.4
20	120.0±3.1	1.3±0.2	55.8±7.9	612±42.1	38.9±10.1	479.9±16.0

The composition of the aerosols detected during the SPR study was investigated for the combustion of mixtures of leaves and fines twigs of branches of cistus, done with the cone calorimeter. The elemental carbon (EC) and organic carbon (OC) contained in the aerosols were quantified. Table 3 summarises the amounts of OC, EC and total carbon produced by the burning of the samples. OC represents 87.23% of the aerosols emitted and the OC/EC ratio is 6.83. Fairly disparate OC/EC values are reported in the literature. They range from 1.2 [50] to 9.6 [51] for forest fuels burned in laboratory experiments. These fuels are of different types including many forest species and grass stands.

Another laboratory study provided OC/EC ratios in between 7.83 and 56 for different forest fuels, with a value of 13.2 for maquis-type fuels [24]. Values greater than unity are common for biomass combustion [51].

Table 3. Quantities of OC and EC (µg) present in the aerosols emitted for the burning of a mixture of leaves and fine twigs.

	Mass (µg)	%
OC	5600	87
EC	820	13
TC	6420	-

3.2. Emission factor according to the thickness of fuel

Based on the phases revealed by the curves of mass, HRR and SPR versus time, the compounds emitted from cistus leaves and twigs were analysed as function of degradation before ignition, flaming and glowing stages. Figure 5 displays emission factors (EF) of the main gases and aerosols emitted during fuel combustion, namely CO_2, CO, nitric oxide (NO) and aerosols (PM). EF are presented as histograms according to the characteristic thickness of the samples. EF_{CO_2} was statistically similar (Table 4, ANOVA, $p > 0.05$) according to diameter of leaves and twigs with an average value of 1540.3 ± 47.9 $g.kg^{-1}$ (all samples combined). The thickness of the twigs has no influence on the EF_{CO_2}, whereas a value of 1666.0 ± 52.0 $g.kg^{-1}$ was obtained by considering only cistus leaves and 1-mm twigs, which have a slightly different composition than those of twigs whose thicknesses are greater than or equal to 2 mm. We note that EF_{CO_2} are in agreement with the literature that reveals total EF_{CO_2} of 1550 ± 95 $g.kg^{-1}$ [15], 1538 ± 125 $g.kg^{-1}$ [24], 1565 ± 128 $g.kg^{-1}$ [36], 1712 ± 66 $g.kg^{-1}$ [52], and 1793 ± 12 $g.kg^{-1}$ [51] (Table 6) in laboratory experiments from various types of biomass burning (savannah and grassland, tropical forest, extratropical forests, biofuel burning, charcoal making, charcoal burning, agricultural residues and amazon forest) and various species (leaves, woody or pine needles from forest fuel). EF_{CO_2} values recorded during field experiments involving maquis-type fires were of the same order of magnitude; i.e., 1478 ± 18 $g.kg^{-1}$ [53], 1684 ± 45 $g.kg^{-1}$ [33], 1700 $g.kg^{-1}$ [30], 814–1752 $g.kg^{-1}$ [54], 1710 ± 39 $g.kg^{-1}$ [19] and 1674 $g.kg^{-1}$ [55] (Table 6).

EF_{CO} was statistically similar (Tab. 4, ANOVA, $p > 0.05$) according to the fuel thickness. The average value of EF_{CO} was found to be 110.0 ± 3.5 g.kg^{-1}. EF_{CO} values reported in the literature show significant variability. Experiments at laboratory scale lead to values of 78 ± 31 g.kg^{-1} [15], 93.2 ± 24.1 g.kg^{-1} [24], 50.3 ± 17.1 g.kg^{-1} [36], and 55.5 ± 7.7 g.kg^{-1} [52], while values recorded during field campaigns (in the case of bush-type fires) are 69.7 ± 6.2 g.kg^{-1} [53], 69 ± 17 g.kg^{-1} [33], 35 g.kg^{-1} [30], 67 ± 13 g.kg^{-1} [19] and 73.8 ± 18.4 g.kg^{-1} [55]] (Table 6). A recent study of Mediterranean maize fires provided CO emission factors in between 51 and 594 g.kg^{-1} [54]. For CO_2 and CO, the experimental burn conditions are over-ventilated. These conditions lead to a good combustion of the fuel leading to stable emission factors as a function of the diameters of the cistus branches.

Emission factors for aerosols EF_a and NO depend on the diameters of the twigs and leaves. EF_a decreases with increasing fuel thickness (ANOVA, $p < 0.05$). This decrease is due to the aerosols emitted during the pre-ignition phase. In fact, during this phase, the aerosol emission factors are the most important. EF_a a is strong for the smallest branch diameters (leaves and branches of 1mm) then they decrease when the diameter of the branches increases. This trend is linked to the mass of fuel degraded during the pre-ignition phase, which increases significantly less than the total mass burned, with the characteristic thickness of the samples. During the flaming phase, the EFs show a slight increase depending on the characteristic thickness (for small branches) of the samples before stabilizing. The aerosol emission factors are more important in the pre-ignition phase than in the flame phase for samples whose thickness is less than or equal to 8 mm. For twigs thicker than 8 mm, the emission factors stabilize for the flame phase and become equivalent to the emission factors in the pre-ignition phase which continue to decrease. To understand this behavior, it is necessary to mention that the duration of the pre-ignition phase is constant for twigs thicker than 5 mm (around 50 s) while the duration of the flame phase increases with thickness of the samples, because the mass of the latter increases. Emission factors in the flame phase are constant for twigs thicker than 8 mm because the mass of fuel burned during this phase increases, as does the total mass of fuel burned. In fact, the mass of aerosols emitted during the flame phase is proportional to the mass of fuel burned, which is considerably greater than the mass lost before ignition. Maximum values were obtained for leaves and 1 mm thick twigs with EF_a of 12.5 ± 3.1 g.kg^{-1} and 13.1 ± 4.0 g.kg^{-1}, respectively. These differences may be the result of variations in the lignocellulosic structures of these fuels compared to the thicker twigs. The lowest value recorded (2.5 ± 0.5 g.kg^{-1}) corresponds to the average emission from samples that are more than 16 mm thick. The average emission factor for aerosols, considering all fuel samples is 4.87 ± 3.11 g.kg^{-1}.

This value is in agreement with the literature, which reports values ranging from 7.2 ± 2.3 g.kg^{-1} [15] to 11.6 ± 6.9 g.kg^{-1} [24, 51] for laboratory experiments. Garcia-Hurtado et al., [54] and Alves et al., [30] provided almost identical values of 3.4 and 3.5 g.kg^{-1} for Mediterranean maquis fires, which are in close agreement with the value of 4.3 g.kg^{-1} reported by Vicente et al., [56] for Mediterranean forest-type vegetation. Recently, the study released of *Pteridium aquilinum L* show the emission factor of aerosols between 9.3 to 14.3 g.kg^{-1} [57]. These values are of same order that those reported for semi-arid scrub fires (7.06 ± 1.5 g.kg^{-1}) [55] and also temperate maquis (9.7 ± 4, 3 g.kg^{-1}) [33] or California forest (7.85 ± 0.55 and 11.9 ± 5.8 g.kg^{-1}) [19, 53]. EF_{NO} decreases with increasing twig diameter (ANOVA, $p < 0.05$). Maximum levels correspond to the burning of leaves with a value of 5.0 ± 0.8 g.kg^{-1} while a value of 1.5 ± 0.3 g.kg^{-1} was obtained for 20 mm twigs, with an average value of 2.4 ± 1.1 g.kg^{-1} when considering the whole set of samples burned. EF_{NO_2} was observed to be independent of the fuel diameter (ANOVA, $p > 0.05$), the average value of $EF_{NO_2}$was 0.2 ± 0.1 g.kg^{-1}. Overall, the average EF of NO_x was found to be 2.5 ± 1.4 g.kg^{-1}, which is in agreement with values reported in the literature. For laboratory-based experiments, EF_{NO_x} values of 1.1 ± 0.6 g.kg^{-1} [15], 2.2 ± 2.2 g.kg^{-1} [24], 2.7 ± 0.8 g.kg^{-1} [36], and 4.4 ± 2.4 g.kg^{-1} [44] have been reported. Field experiments provided EF_{NO_x} values of 0.3 g.kg^{-1} [30], 3.3 ± 1.0 g.kg^{-1} [19] and 2.2 ± 0.8 g.kg^{-1} [55]] (Table 6).

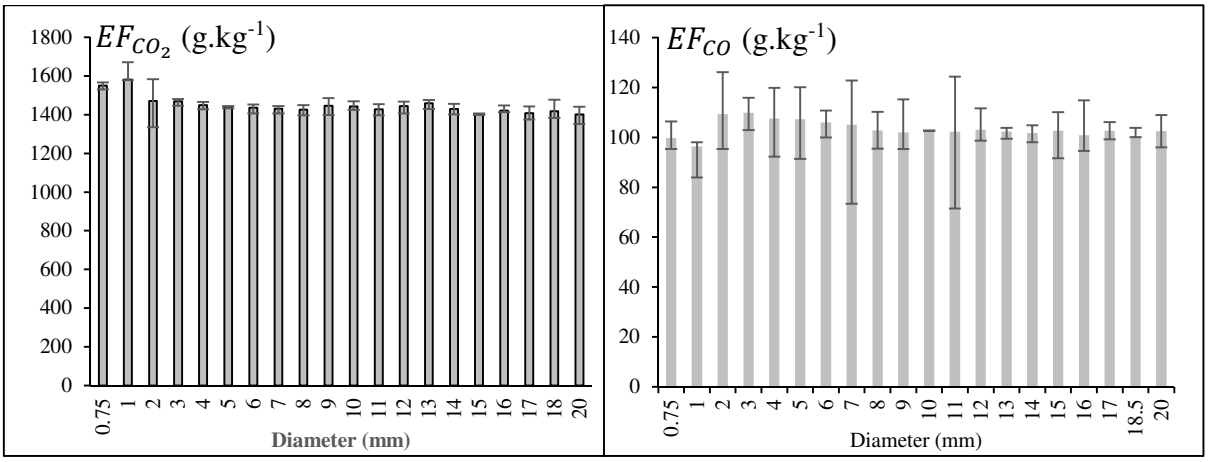

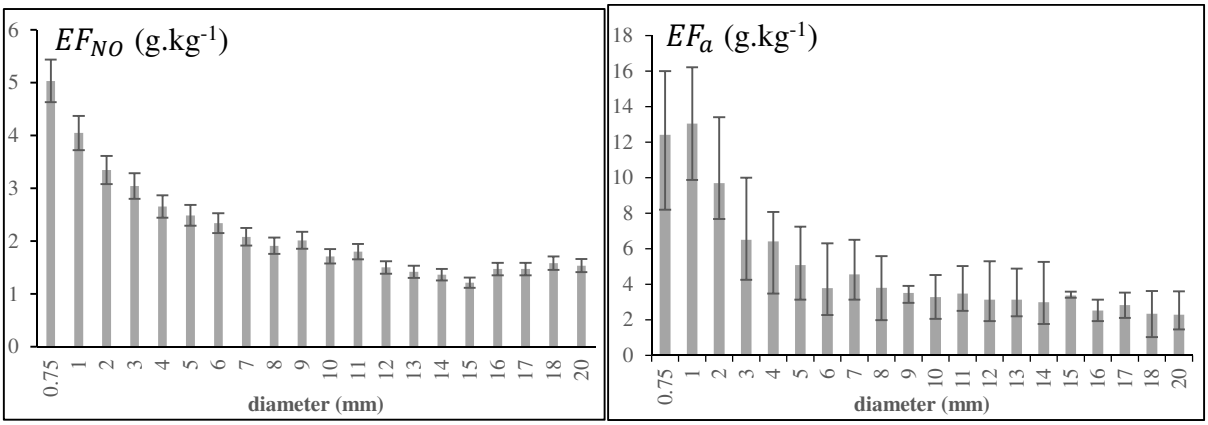

Figure 5. Emission factors of the main constituents (EF_i) according to the fuel thickness (EF_{CO_2}: emission factor of CO_2; EF_{CO} : emission factor of CO; EF_{NO} : emission factor of CO and EF_a : emission factor of aerosols).

Table 4 shows EF values of compounds analysed as functions of the fuel thickness. For the major part of the compounds i.e. CO_2, H_2O, CO, NH_3, C_3H_8, C_5H_{12}, NO_2 and VOC, the EF were statistically similar and irrespective of the thickness of the fuel. As seen previously, the EF of aerosols decreases with the thickness of fuel (ANOVA, $p < 0.05$). To understand this behavior, it is necessary to mention that the duration of the pre-ignition phase (see Table 2) is constant for twigs thicker than 5 mm (around 50 s). It was observed that the aerosol content in the pre-ignition phase is more important for the leaves and twigs of 1 mm. For the finest diameters, the radiant heat flux allows to heat and degrade all the mass within the fuel and therefore the aerosols are emitted across the entire surface of the samples. For this thermally-thin pyrolysis regime, EF of aerosol is greater than for the thick particles. When the fuel diameter increases, only the vicinity of the upper face of the fuel (exposed to the heater) undergoes degradation. Aerosols are therefore emitted by the upper face and the EF of aerosol decreases (thermally-thick pyrolysis regime).

The limit size in between thermally thin and thick regimes correspond to a thickness of 5 mm. The EF of NO, formaldehyde and methane decrease with the fuel thickness (ANOVA, $p < 0.05$). In general, the production of NO increases when the temperature increases. Flames with fine particles are more powerful (see HRR in Fig. 4). The temperature is certainly higher which promotes the production of NO. Then as the flames are less powerful, the temperature is less important which leads to less production of NO. The EF of VOC (quantified with ATD-GC/MS) were statistically similar when the thickness increases (Tab. 4).

Table 4. Average EF ($g.kg^{-1}$) during the combustion of samples according to the fuel thickness (Statistical analysis of compounds according to the fuel thickness; a, b, c and d: significant difference among diameter of twigs; with a > b > c > d > e).

Diameter	CO_2	CO	PM	H_20	CH_4	NO	NO_2	NH_3	C_3H_8	C_5H_{12}	CH_2O	VOC* ($mg.kg^{-1}$)
0.75	1649±51^{a}	106.0±6.3^{a}	12.5±3.1^{a}	587±43^{a,b}	1.03±0.2^{a}	5.0±0.8^{a}	0.4^{a}	2.4^{a}	0.3^{a}	0.15^{a}	0.07^{a}	428.3±32^{a}
1	1683±55^{a}	102.5±7.8^{a}	13.1±4.0^{a}	611±33^{a}	0.23±0.0^{b}	4.3±0.3^{b}	0.3^{a}	0.2^{b}	0.2^{a}	0.14^{a}	0.07^{a}	350.5±65^{a}
2	1565±65^{a}	116.3±8.1^{a}	9.7±3.7^{a,b}	529±68^{a,b}	0.22±0.0^{b}	3.6±0.3^{c}	0.2^{a}	0.3^{b}	0.4^{a}	0.27^{a}	0.09^{a}	385.5±55^{a}
3	1563±13^{a}	116.8±3.7^{a}	6.5±3.5^{a,b}	540±26^{b}	0.21±0.0^{b}	3.2±0.2^{c}	0.2^{a}	0.3^{b}	0.2^{a}	0.17^{a}	0.05^{a,b}	481.9±42^{a}
4	1541±17^{a}	114.4±6.1^{a}	6.4±1.7^{a,b}	498±21^{b}	0.22±0.0^{b}	2.8±0.1^{c,d}	0.2^{a}	0.2^{b}	0.2^{a}	0.16^{a}	0.05^{a,b}	530.1±95^{a}
5	1530±27^{a}	114.1±11.9^{a}	5.1±2.2^{b}	500±57^{b}	0.25±0.0^{b}	2.7±0.3^{c,d}	0.2^{a}	0.3^{b}	0.2^{a}	0.16^{a}	0.05^{a,b}	475.5±66^{a}
6	1528±25^{a}	112.8±9.8^{a}	3.8±2.5^{b}	485±45^{b}	0.30±0.0^{b}	2.5±0.2^{d}	0.2^{a}	0.2^{b}	0.3^{a}	0.15^{a}	0.04^{a,b}	385.5±65^{a}
7	1523±20^{a}	111.8±5.9^{a}	4.8±1.9^{b}	502±46^{b}	0.33±0.0^{b}	2.2±0.3^{d}	0.2^{a}	0.2^{b}	0.2^{a}	0.13^{a}	0.04^{a,b}	506.2±110^{a}
8	1518±22^{a}	109.4±18.1^{a}	3.8±1.8^{b}	482±20^{b}	0.30±0.0^{b}	2.0±0.3^{d}	0.2^{a}	0.2^{b}	0.2^{a}	0.11^{a}	0.03^{b}	350.5±65^{a}
9	1538±36^{a}	108.5±7.5^{a}	3.5±0.4^{b}	478±53^{b}	0.29±0.0^{b}	2.1±0.2^{d}	0.1^{a}	0.2^{b}	0.2^{a}	0.10^{a}	0.03^{b}	385.5±22^{a}
10	1535±42^{a}	109.2±8.2^{a}	3.3±1.2^{b}	467±12^{b}	0.31±0.0^{b}	1.8±0.3^{d}	0.1^{a}	0.2^{b}	0.1^{a}	0.08^{a}	0.02^{b}	481.9±55^{a}
11	1520±23^{a}	108.8±11.4^{a}	3.5±1.5^{b}	484±11^{b}	0.33±0.0^{b}	1.9±0.2^{d}	0.1^{a}	0.2^{b}	0.2^{a}	0.08^{a}	0.02^{b}	433.7±85^{a}
12	1536±32^{a}	109.6±18.6^{a}	3.1±1.2^{b}	464±25^{b}	0.29±0.0^{b}	1.6±0.2^{d,e}	0.1^{a}	0.2^{b}	0.2^{a}	0.06^{a}	0.02^{b}	390.3±55^{a}
13	1553±44^{a}	108.8±11.8^{a}	3.1±0.2^{b}	456±32^{b}	0.34±0.0^{b}	1.5±0.2^{d,e}	0.2^{a}	0.2^{b}	0.1^{a}	0.03^{a}	0.02^{b}	351.3±39^{a}
14	1521±25^{a}	108.2±11.2^{a}	3.0±01.7^{b}	481±19^{b}	0.30±0.0^{b}	1.5±0.2^{d,e}	0.1^{a}	0.2^{b}	0.2^{a}	0.05^{a}	0.02^{b}	361.3±44^{a}
15	1492±28^{a}	109.2±7.5^{a}	3.4±1.7^{b}	485±44^{b}	0.38±0.0^{b}	1.3±0.2^{d,e}	0.2^{a}	0.1^{b}	0.2^{a}	0.09^{a}	0.03^{b}	393.4±52^{a}
16	1513±8^{a}	107.2±9.9^{a}	2.5±0.5^{b}	487±16^{b}	0.46±0.1^{b}	1.7±0.4^{d}	0.2^{a}	0.2^{b}	0.2^{a}	0.07^{a}	0.03^{b}	396.4±53^{a}
17	1499±27^{a}	109.2±12.8^{a}	2.8±0.8^{b}	494±14^{b}	0.45±0.1^{b}	1.6±0.3^{d}	0.2^{a}	0.2^{b}	0.2^{a}	0.07^{a}	0.03^{a}	351.3±85^{a}
18	1499±57^{a}	108.2±11.3^{a}	2.5±1.2^{b}	499±22^{b}	0.47±0.1^{b}	1.6±0.4^{d}	0.2^{a}	0.2^{b}	0.2^{a}	0.06^{a}	0.02^{a}	475.5±102^{a}
19	1509±14^{a}	106.3±7.6^{a}	2.5±1.3^{b}	505±27^{b}	0.42±0.1^{b}	1.6±0.3^{d}	0.2^{a}	0.2^{b}	0.1^{a}	0.04^{a}	0.02^{a}	385.5±81^{a}
20	1490±22^{a}	109.1±7.8^{a}	2.5±1.0^{b}	497±21^{b}	0.55±0.1^{b}	1.5±0.3^{d}	0.2^{a}	0.2^{b}	0.1^{a}	0.06^{a}	0.02^{a}	350.5±77^{a}

*For NO_2, NH_3, C_3H_8, C_5H_{12} and CH_2O, the standard deviation is less than 0.1, *: Total VOC quantified in the ATD-GC/MS.*

Table 5 lists the 30 compounds identified in smoke in our experiments and the corresponding mean EF. CO_2, H_2O, CO, and aerosols are the main compounds emitted in smoke, while NOx (mainly NO and smaller amounts of NO_2), CH_4, and NH_3 were observed in smaller proportions. The emission factors were averaged for all the samples by combining the data from twigs of all diameters. The values obtained for EF_{CH_4} (0.5 ± 0.2 $g.kg^{-1}$) and EF_{NH_3} (0.3 ± 0.5 $g.kg^{-1}$) are lower than that observed in the literature. For laboratory experiments, EF_{CH_4} values of 2.5 ± 2.1 $g.kg^{-1}$ [24], 1.2 ± 0.8 $g.kg^{-1}$ [52], and 0.9 ± 0.3 $g.kg^{-1}$ [51] have been reported (Table 6).

For field experiments, the following values of EF_{CH_4} were given: 2.8 ± 0.6 g.kg^{-1} [53], 2.3 ± 1.1 g.kg^{-1} [33], 1.4 g.kg^{-1} [30], 2.5 ± 0.7 g.kg^{-1} [19] and 3.7 ± 1.4 g.kg^{-1} [55]. EF_{NH_3} values of 1.3 g.kg^{-1} [15], 1.5 ± 1.3 g.kg^{-1} [24], and 0.2 ± 0.1 g.kg^{-1} [52] were obtained at laboratory scale and EF_{NH_3} values of 1.3 g.kg^{-1} [30], 1.03 ± 0.7 g.kg^{-1} [19], and 1.5 ± 1.4 g.kg^{-1} [55] were obtained for maquis-type fires (Table 6). Benzene is the main VOCs emitted except the linear hydrocarbons, with an emission factor between of 113.8 ± 11.2 mg.kg^{-1}. This result is consistent with the laboratory-scale results of Santoni et al., [44] with 98 ± 3 mg.kg^{-1}, Barboni et al., [48] with 123.6 ± 35.5 mg.kg^{-1}, and Aurell et al., [51] with 92 ± 20 mg.kg^{-1}. On the other hand, this value is somewhat lower than those reported by Urbanski et al., [33] (220 mg.kg^{-1}) and Yokelson et al., [55] (451 ± 287 mg.kg^{-1}) for temperate and semi-arid scrub fires. TEXS (toluene, ethylbenzene, xylenes, and styrene) are also present in smoke, as are furan and its derivatives, with respectively EF in the ranges of [54.2–118.7] mg.kg^{-1} and [7.4–82.9] mg.kg^{-1} as function of fuel thickness. We also note the presence of naphthalene (a volatile PAH) in low proportions.

Table 5. Average EFs (g.kg^{-1}) of compounds identified in smoke emitted during the combustion of fuel samples.

N°	Compounds	
	IRND	EF (g.kg^{-1})
1	CO_2 (carbon dioxide)	1540 ± 48
2	CO (carbon monoxide)	110.0 ± 3.5
	Laser He-Ne	
3	Aerosols	4.9 ± 3.1
	FTIR	
4	H_2O (water)	502.1 ± 38.7
5	CH_4 (methane)	0.36 ± 0.18
6	C_3H_8 (propane)	0.20 ± 0.06
7	C_5H_{12} (pentane)	0.11 ± 0.06
8	CH_2O (formaldehyde)	0.04 ± 0.02
9	NO (nitrogen monoxide)	2.35 ± 1.06
10	NO_2 (nitrogen dioxide)	0.19 ± 0.06
11	NH_3 (ammonia)	0.31 ± 0.50
	ATD/GC-MS	EF (mg.kg^{-1})
12	C_3H_6 (propene)	10.3 ± 17.4
13	C_6H_{14} (hexane)	59.6 ± 38.4
14	C_7H_{16} (heptane)	1.3 ± 1.7

15	C_6H_6 (benzene)	113.8 ± 51.2
16	C_7H_8 (toluene)	16.7 ± 8.4
17	C_8H_{10} (ethylbenzene)	17.1± 8.9
18	C_8H_{10} (xylene)	9.4 ± 4.4
19	C_8H_8 (styrene)	11.0± 9.1
20	C_7H_6O (benzaldehyde)	9.8± 7.4
21	C_6H_6O (phenol)	7.8± 8.4
22	C_4H_5N (pyrrole)	6.8 ± 5.8
23	C_5H_6O (methyl-furan)	25.8 ± 31.9
24	C_6H_8O (dimethylfuran)	9.3 ± 14.1
25	$C_5H_4O_2$ (furfural)	47.8 ± 51.2
26	C_8H_6 (phenylethyne)	12.6 ± 9.0
27	$C_7H_{14}O$ (heptanal)	10.5 ± 15.3
28	$C_4H_6O_2$ (diacetyl)	13.0 ± 23.4
29	$C_2H_4O_2$ (acetic acid)	6.9 ± 11.4
30	$C_{10}H_8$ (naphthalene)	2.9 ± 2.4

The CO and CO_2 measurements were used to calculate the modified combustion efficiency (MCE). A mean value of 0.93 was obtained (using equation 6 on the whole phases of combustion and all the samples burned) which indicates that the flame phase predominates. Our experiments reveal that the combustion is over-ventilated with the calorimeter cone. It is consistent with the fact that a significant amount of mass (close to 82%) is lost during the flaming phase (Fig. 3). MCE values have been reported for other studies on Mediterranean forest fires. Evtuygina et al., [31] reported a value of 0.82 ± 0.08, while Alves et al., [30] provided values between 0.6 and 0.86. In order to improve our understanding of the dynamics of phase emissions, we determined the chemical composition of smoke as a function of combustion phase; i.e., before ignition, during flaming and during the glowing phase.

Table 6. Emission factors ($g.kg^{-1}$) measured for different types of vegetation

Chemical species	Forest[a]	Maquis[b]	Savannah[c]	Laboratory[d]
CO_2	1377 – 1737	854 – 1752	1613 – 1700	1311 – 1793
CO	55.5 – 231	35 – 453	63 – 79	24 – 96.4
CH_4	3.4 – 9.2	1.4 – 46	1,7 – 4.1	0.9 – 6.1
VOC	0.39 – 23.2	7.1 – 8.9	2.7 – 3.4	7.3 – 14.2
NO_x	0.5 – 4.6	0.3 – 3.3	2.3 – 6	1.1 – 7.45
Aerosol	4.3 – 19.3	3.4 – 11.9	2.7 – 7.7	0.8 – 29.4
OC	4.5 – 15.8	1.4 – 6.2	2.3 – 3.4	4 – 18.4
BC	0.0087 – 0.62	0.051 – 1.3	0.37 – 0,5	0.1 – 4.4

Benzene	0.27 – 1.1	0.451	0.18 – 0.23	0.013 – 1.9
Toluene	0.22 – 0.48	–	0.08 – 0.15	0.019 – 1.1
NH_3	0.4 – 2.72	1.03 – 1.5	0.26 – 1.5	0.237 – 2.7
CH_2O (formaldehyde)	1.66 – 2.76	0.83 – 1.33	0.26 – 1.1	0.13

[15][d]; [53][b]; [25][c]; [15][a,c,d]; [26][c]; [24][d]; [27][a]; [33][a,b,c]; [30][b]; [19][a,b,c]; [18][a]; [36][d]; [34][a,c]; [31][a]; [54][b]; [55][b]; [45][d]; [51][d]; [29][a]; [52][d]; [56][b]; [44][d]; [48][d]; [57][d];

3.3. Production rates of species according to the phases of degradation and combustion

Figures 6 and 7 show the rates of production of the main gaseous compounds and aerosols emitted over time for two twigs typical of the thermally fine and thermally thick regimes of pre-heating. The profiles of the rates of production in both figures are similar with respect to the pre-ignition and glowing phases. During the flame phase, two previously described characteristic peaks were observed in the flame phase HRR curves (Fig. 4) for thick samples while for a finer fuel thickness, a single peak of HRR was observed. The phases of pre-ignition, flaming and glowing after the flameout are delimited by vertical lines in Figures 6 and 7.

The emission factors corresponding to theses phases were determined for the main compounds and are provided in Table 7. The data corresponding to averages for all fuel thicknesses. CO_2 is mainly emitted (69%) during the flaming phase and to a lesser extent (30%) during the glowing phase. For cistus leaves and twigs with thicknesses less than or equal to 4 mm, the CO_2 emission was observed to increase slightly during the pre-ignition and flame phases, and decrease slightly during the glowing phase, with increasing sample thickness. CO was mainly emitted (91%) during the glowing phase for all samples. During the pre-ignition and flaming phases the production rates are low and constant for all fuel samples. Aerosols are mainly emitted during the pre-ignition phase, at 95% for leaves and twigs with 1 and 2 mm diameter, and at an average of 76% for all other fuel thicknesses. Aerosols are one of the major components emitted during the pre-ignition phase with CO_2 and H_2O. Without CO_2 and H_2O, aerosol represent 98% of smoke composition for leaves and 1 mm diameter twigs, and 61% for twigs thicker than 1 mm. NO is emitted mainly during the flaming phase (up to 67%) and represents 0.08% of the gases emitted for all diameter fuels. NH_3 and CH_4 are mainly emitted during the glowing phase, at 86% and 69%, respectively. They are produced at average values of 0.2% (2.5% for the leaves) and 0.3% (0.9% for leaves) of the gases emitted when fuels of all diameters are combined. VOCs were also measured according to the burning phases. It is noted that VOCs are almose present in the flame phase. Very small quantities are identifiable during the pre-ignition phase but not quantifiable.

To be able to identify and quantify these VOCs during the pre-ignition phase, it would be necessary to reduce the smoke extraction of the cone calorimeter exhaust duct, which would allow an enrichment of the captured VOCs.

These results highlight the importance of distinguishing the emissions of the various constituents as functions of the burning phases for emission models. They make it potentially possible to predict pollutant emissions when evaluating the exposure to smoke of people near contact with fire. They can be used for dispersion models or coupled fire-atmosphere models as input for predicting the dispersion of pollutants at short and long distances from a fire in order to warn firefighters and population in case of chemical risk.

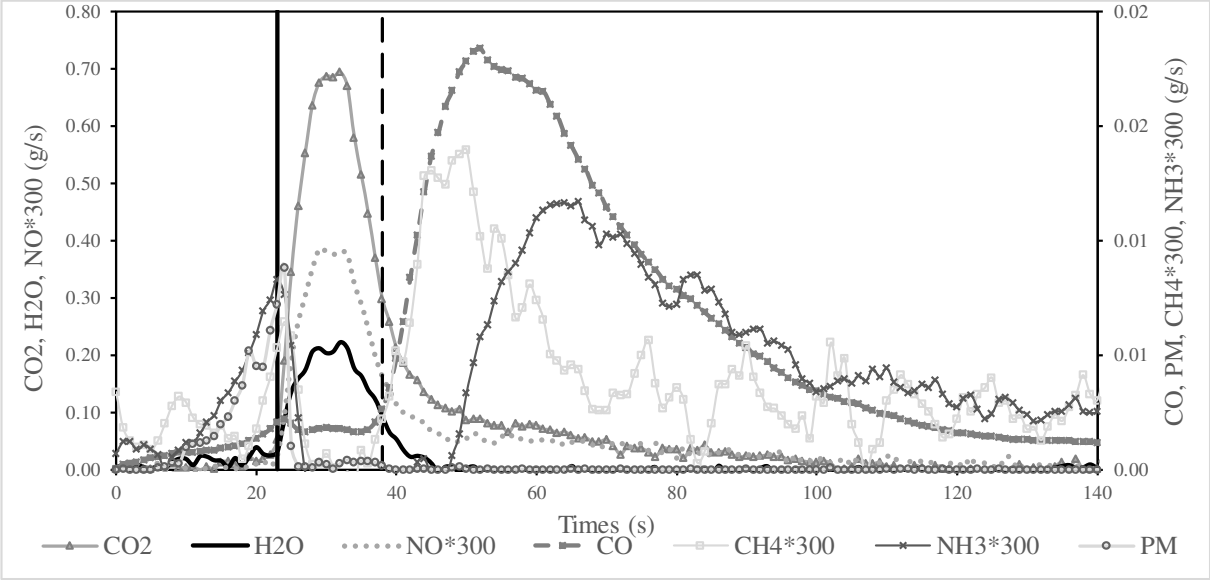

Figure 6. Production rates of the main gases and PM over time for the burning of 2 mm twigs diameter (The vertical lines represent ignition and flameout times).

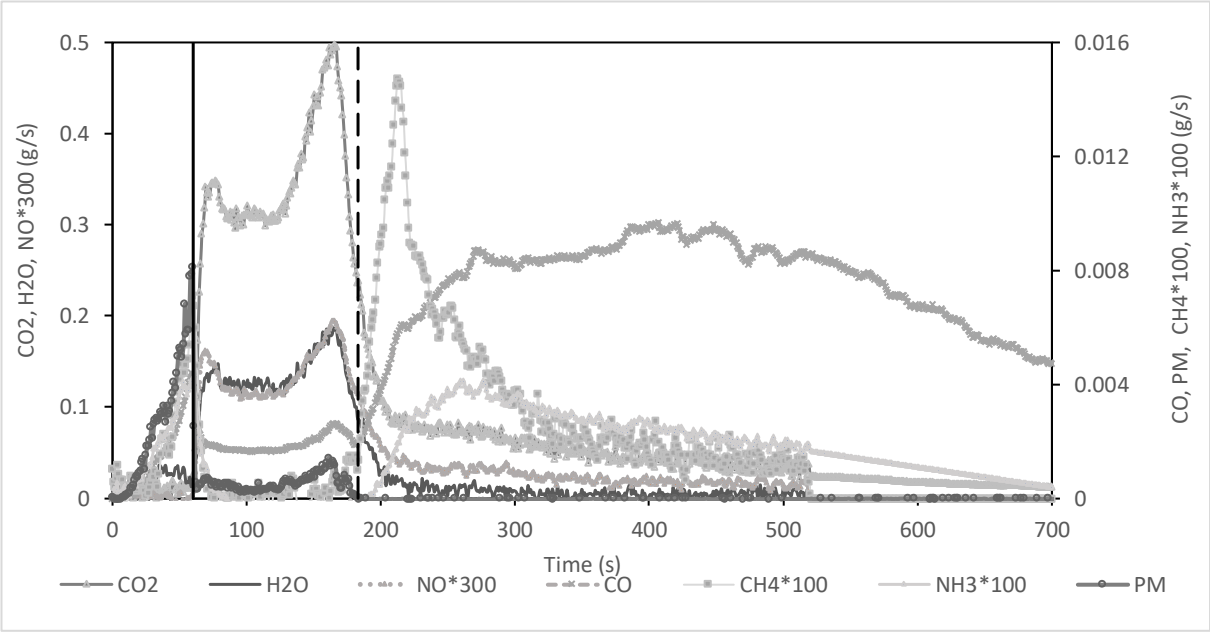

Figure 7. Production rates of the main gases and aerosols over time for the burning of 8 mm twigs diameter (the vertical lines represent ignition and flameout times).

Table 7. EF averages for all fuel thickness ($g.kg^{-1}$) according to combustion phase.

N°	Compounds			
	Analyzed with NDIR	Pre-ignition	Flame	Glowing
1	CO_2 (carbon dioxide)	15.6 ± 23.3	1072.8 ± 79.8	454.3 ± 51.3
2	CO (carbon monoxide)	1.0 ± 0.4	8,59 ± 1.9	100.0 ± 4.1
	Measured with Laser He-Ne	Pyrolyse	Flame	Glowing
3	Aerosols	3.6 ± 3.2	1.3 ± 0.4	–
	Analyzed with FTIR	Pyrolyse	Flame	Glowing
4	H_2O (water)	23.8 ± 18.3	427.6 ± 20.3	50.7 ± 24.3
5	CH_4 (methane)	0.02 ± 0.01	0.08 ± 0.04	0.3 ± 0.2
6	C_3H_8 (propane)	0.05 ± 0.04	0.04 ± 0.01	0.1 ± 0.04
7	C_5H_{12} (pentane)	0.03 ± 0.03	0.04 ± 0.02	0.04 ± 0.03
8	CH_2O (formaldehyde)	0.01 ± 0.01	0.01 ± 0.01	0.02 ± 0.01
9	NO (nitrogen oxide)	0.02 ± 0.02	1.6 ± 0.7	0.7 ± 0.4
10	NO_2 (nitrogen dioxide)	0.01 ± 0.01	0.1 ± 0.02	0.08 ± 0.05
11	NH_3 (ammonia)	0.02 ± 0.01	0.01 ± 0.01	0.3 ± 0.5

729 *3.4. Carbon mass balance*

730 Analyses of the products from fuel combustion reveal numerous carbon compounds. We
731 determined the carbon mass balance (CMB) in order to assess the quality of our analyses, the
732 results of which are summarised in Table 8. The CMB provides a comparison between the
733 amount of carbon present in the smoke and the one available in the fuel, as determined by the
734 elemental analyses given in Table 1. The cistus twigs produced 493.2 $g_C.kg^{-1}$ (grams of carbon
735 per kilogram of fuel), while leaves produced 485.0 $g_C.kg^{-1}$. The total CMB was calculated by
736 summing the carbon identified in the gas and particulate phases (tars and soot). As reported
737 previously [49], the major compound present in tars is levoglucosan. Consequently, we
738 assumed that the tars were entirely composed of levoglucosan when determining the CMB of
739 the tars, while the soot particles were assumed to be pure carbon. The CMB allows to asses that
740 96% of the carbon potentially emitted was analysed. The average remaining ash (when
741 considering all samples and all size of particles) represents 2% of the initial mass the samples.
742

743 Table 8. Carbon mass balances ($g_C.kg^{-1}$) during fuel combustion with the cone calorimeter.

compounds	
NDIR	Cistus fuel
CO_2 (carbon monoxide)	420 ± 13
CO (carbon dioxide)	47.1 ± 1.5
Laser He-Ne	
tars ($C_6H_{10}O_5$: levoglucosan)	1.6 ± 1.4
soot	1.3 ± 0.4
FTIR	
CH_4 (methane)	0.27 ± 0.13
C_3H_8 (propane)	0.16 ± 0.05
C_5H_{12} (pentane)	0.09 ± 0.05
CH_2O (formaldehyde)	0.02 ± 0.01
ATD/GC-MS	
C_3H_6 (propene)	0.01 ± 0.001
C_6H_{14} (hexane)	0.05 ± 0.01
C_7H_{16} (heptane)	0.001 ± 0.001
C_6H_6 (benzene)	0.11 ± 0.01
C_7H_8 (toluene)	0.015 ± 0.003
C_8H_{10} (ethyl-benzene)	0.015 ± 0.002
C_8H_{10} (xylenes)	0.009 ± 0.002
C_8H_8 (styrene)	0.010 ± 0.005
C_7H_6O (benzaldehyde)	0.008 ± 0.003
C_6H_6O (phenol)	0.006 ± 0.003

C_4H_5N (pyrrole)	0.006 ± 0.003
C_5H_6O (methyl-furan)	0.02 ± 0.01
C_6H_8O (dimethyl-furan)	0.007 ± 0.003
$C_5H_4O_2$ (furfural)	0.03 ± 0.01
C_8H_6 (phenylethyne)	0.012 ± 0.001
$C_7H_{14}O$ (heptanal)	0.008 ± 0.004
$C_4H_6O_2$ (diacetyl)	0.007 ± 0.002
$C_2H_4O_2$ (acetic acid)	0.004 ± 0.001
$C_{10}H_8$ (naphthalene)	0.003 ± 0.002
Total carbon mass balance (smoke)	**471 ± 17**
Carbon total (elemental analyses)	**493**
% of Carbon recovered	**96 %**

Conclusion

The chemical compounds emitted during the combustion of cistus leaves and twigs were studied with a cone calorimeter. 96 % of the carbon emitted in the smoke was recovered by comparison with the carbon content of the fuel. The emission factors for aerosols, carbonaceous, water and nitrogenous compounds were determined by analytical methods. The main conclusions can be summarized as follows:

1. The greater mass loss was observed during the flame phase for the burning of cistus leaves and twigs. The MCE has been calculated and indicates that the flame phase is predominant in our experiments with a cone calorimeter and a ventilated holder. The loss of mass during the flame phase is mainly converted into CO_2.
2. CO_2, CO, aerosols, and NO were the major pollutants emitted, with emission factors on the order of 1600 $g.kg^{-1}$ and 100 $g.kg^{-1}$ for CO_2 and CO, respectively. Organic carbon (OC) were present in the aerosols at higher levels than elemental carbon (EC). Their ratio was 6.83 for cistus fuel (leaves and fine twigs).
3. Emission factors of CO_2 and CO were independent of twigs diameter and cistus fuel type (twigs or leaves), while the emission factors of aerosols and NO decreased with increasing twigs diameter.

4. The rate of production and emission factors of gases and aerosols during the various combustion phases, namely pre-ignition, flaming and glowing phases were determined. Aerosols were mainly emitted during the pre-ignition phase, while CO_2, H_2O, and NO were mainly emitted during the flame phase. CO, CH_4, and NH_3 were mainly emitted during the glowing phase.

5. The data presented in this work make it possible to determine the parameters that are integrated into coupled simulation models propagation / atmosphere, in order to provide decision support for the management of fire risks. On a demonstration of the influence of the size of vegetable particles on flammability, a more precise representation of smoke emissions, in particular with regard to aerosols and their dispersion. The distinction according to the combustion phases makes it possible to simulate the impact of the smoke on people near fire. Indeed, the emission of pollutants during the pre-ignition and flaming phases are those directly impacting the personnel involved. These studies must be carried out on different fuels, making it possible to determine the pollutants emitted as well as the combustion size limit according to the fuel studied.

References

[1] Food and Agriculture Organization of the United Nations (2007) Fire management global assessment 2006, progress towards sustainable forest management. Rome.

[2] Prométhée (2018) La banque de données sur les incendies de forêts en région Méditerranéenne en France. http://www.promethee.com/.

[3] D.E. Ward, Characteristic emission of smoke from prescribed fires for source apportionment. the 23rd Annual meeting. Eugene, Oregon, 1986, 160-166.

[4] WHO. 2014. 7 millions de décès prématurés sont liés à la pollution de l'air chaque année. WHO Regional Office for Europe, Genève.

[5] B.B. Langmann, C. Duncan, J. Textor, Trentmann, et G.R. Van der Werf. Vegetation fire emissions and their impact on air pollution and climate. Atmos. Environ. 43 (2009) 107-116.

[6] J.S. Lighty, J.M. Veranth, A.F. Sarofim, Combustion aerosols: factors governing their size and composition and implications to human health. Journal of the Air and Waste Management Association 50, 1565-1618. Mandel, J., Beezley, D.J., Kochanski, A., 2011. An overview of the coupled atmosphere-wildland fire model WRF-Fire. 91st American Meterological Society Annual Meeting, Seattle, WA, 2000.

[7] A.J. Cohen, H.R. Anderson, B. Ostro, K.P. Pandev, M. Krzyzanowski, N. Künzli, K. Gutschmidt, A. Pope, I. Romieu, J.M. Samet, K. Smith, The global burden of disease due to outdoor air pollution. J. Toxicol. Env. Health 68 (2005) 1301-1307.

[8] WHO. Health risks of particulate matter from lon-range transboundary air pollution. Copenhague: WHO Regional Office for Europe, 2006.

[9] CPRIM, Cohorte. 2011. Analyse de la mortalité des sapeurs-pompiers professionnels actifs au 1er janvier 1979. Rapport scientifique, Bordeaux, in French.

[10] A.I. Miranda, An integrated numerical system to estimate air quality effects of forest fires. Inter. J. Wildland Fire 13 (2004) 217–226.

[11] A.I. Miranda, J. Ferreira, J. Valente, P. Santos, J.H. Amorim, C. Borrego, Smoke measurements during Gestosa-2002 experimental field fires. Inter. J. Wildland Fire 14 (2005) 107–116.

[12] M. Statheropoulos, S. Karma, Complexity and origin of the smoke components as measured near the flame-front of a real forest fire incident: A case study. J.Anal. Appl. Pyrol 78 (2007) 430-437.

[13] I. Dokas, M. Statheropoulos, S. Karma, Integration of field chemical data in initial risk assessment of forest fire smoke. Sci. Total Environ. 376 (2007) 72-85.

[14] T. Barboni, M. Cannac, V. Pasqualini, A. Simeoni, E. Leoni, N. Chiaramonti, Volatile and semi-volatile organic compounds in smoke exposure of firefighters during prescribed burning in the Mediterranean region. Int. J. Wildland Fire 19 (2010) 606-612.

[15] M.O. Andreae, P. Merlet, Emission of trace gases and aerosols from biomass burning. Global Biogeochemical Cycles 15 (2001) 955-966.

[16] P. Ciccioli, E. Brancaleoni, M. Frattoni, A. Cecinato, L. Pinciarelli, Determination of volatile organic compounds (VOC) emitted from biomass burning of Mediterranean vegetation species by GC-MS, Anal. Lett. 34 (2001) 937-955.

[17] H.R. Friedli, E. Atlas, V.R. Stroud, L. Giovanni, T. Campos, L.F. Radke, Volatile organic trace gases emitted from North American wildfires, Global Biogeochem. Cycles 15 (2001) 435-452.

[18] I.J. Simpson, S.K. Akagi, B. Barletta, N.J. Blake, Y. Choi, G.S. Diskin, A. Fried, H.E. Fuelberg, S. Meinardi, F.S. Rowland, S.A. Vay, A.J. Weinheimer, P.O. Wennberg, P. Wiebring, A. Wisthaler, M. Yang, R.J. Yokelson, D.R. Blake, Boreal forest fire emissions in fresh Canadian smoke plumes: C_1-C_{10} volatile organic compounds (VOC_s), CO_2, CO, NO_2, NO, HCN and CH_3CN. Atmos. Chem. Phys. 11 (2011) 6445-6463.

[19] S.K. Akagi, R.J. Yokelson, C. Wiedinmyer, M.J. Alvarado, J.S. Reid, T. Karl, J.D. Crounse, P.O. Wennberg, Emission factors for open and domestic biomass burning for use in atmospheric models. Atmos. Chem. Phys 11 (2011) 4039-4072.

837 [20] M. Evtyugina, A. Alves, T. Nunes, L. Tarelho, M. Duarte, S.O. Prozil, C. Pio, VOC
838 emissions from residential combustion of Southern and mid-European woods. Atmos.
839 Environ. 83 (2014) 90-98.

840 [21] J.B. Gilman, B.M. Lerner, W.C. Kuster, P.D. Goldan, C. Warneke, P.R. Veres, J.M.
841 Roberts, J.A. de Gouw, I.R. Burling, R.J. Yokelson, Biomass burning emissions and
842 potential air quality impacts of volatile organic compounds and other trace gases from
843 fuels common in the US, Atmos. Chem. Phys. 15 (2015) 13915-13938.

844 [22] L.E. Hatch, R.J. Yokelson, C.E. Stockwell, P.R. Veres, I.J. Simpson, D.R. Blake, J.J.
845 Orlando, K.C. Barsanti, Multi-instrument comparison and compilation of non-methane
846 organic gas emissions from biomass burning and implications for smoke-derived
847 secondary organic aerosol precursors, Atmos. Chem. Phys. 17 (2017) 1471-1489.

848 [23] J.S. Reid, R. Koppmann, T.F. Eck, D.P. Eleuterio, A review of biomass burning
849 emissions part II: intensive physical properties of biomass burning particles. Atmos.
850 Chem. Phys. 5 (2005) 799-825.

851 [24] G.R. McMeeking, S.M. Kreidenweis, S. Baker, C.M. Carrico, J.C. Chow, J.L. Collett,
852 W.M. Hao, A.M. Holden, T.W. Kirchstetter, W.C. Malm, H. Moosmüller, A.P.
853 Sullivan, C.E. Wold, Emission of trace gases and aerosols during the open combustion
854 of biomass in the laboratory. J. Geophysical Res. 114, D19210, 2009.

855 [25] D.E. Ward, W.M. Hao, R.A. Susott, R.E. Babbitt, R.W. Shea, J.B. Kauffman, Justice
856 C.O., Effect of fuel composition on combustion efficiency and emission factors for
857 african savanna ecosystems. J. geophysical Res. 101 (1996) 23569-23576.

858 [26] P. Sinha, P.V. Hobbs, R.J. Yokelson, I.T. Bertschi, D. R. Blake, I.J. Simpson, S. Gao,
859 T.W. Kirchstetter, T. Novakov, Emissions of trace gases and particles from savanna
860 fires in southern Africa. J. Geophysical Res. 108 (2003) 8487.

861 [27] T.G. Soares Neto, J.A Jr. Carvalho, C.A.G. Veras, E.C. Alvarado, R. Gielow, E.N.
862 Lincoln, T.G. Christian, R.J. Yokelson, J.C. Santos, Biomass consumption and CO_2,
863 CO and main hydrocarbon gas emissions in an Amazonian forest clearing fire. Atmos.
864 Environ. 43 (2009) 438-446.

865 [28] S.P. Urbanski, Combustion efficiency and emission factors for wildfire-season fires in
866 mixed conifer forests of the northern Rocky Mountains, US. Atmos. Chem. Phys. 13
867 (2013) 7241-7262.

868 [29] J. Aurell, B. Gullett, D. Tabor, N. Yonker, Emissions from prescribed burning of timber
869 slash piles in Oregon. Atmos. Environ. 150 (2017) 395-406.

870 [30] C.A. Alves, C. Gonçalves, C.A. Pio, F. Mirante, A. Caseiro, L. Tarelho, M.C. Freitas,
871 D.X. Viegas, Smoke emissions from biomass burning in a Mediterranean shrubland.
872 Atmos. Environ. 44 (2010) 3024-3033.

[31] M. Evtuygina, A.I. Calvo, T. Nunes, A. Alves, P. Fernandes, L. Tarelho, A. Vicente, C. Pio, VOC emissions of smoldering combustion from Mediterranean wildfires in central Portugal. Atmos. Environ. 64 (2013) 339-348.

[32] F. Reisen, S.K. Brown, Australian firefighters' exposure to air toxics during bushfire burns of autumn 2005 and 2006. Environ. Int. 35 (2009) 342-352.

[33] S.P. Urbanski, W.M. Hao, S. Baker, Chemical composition of wildland fire emissions. Dans Developments in Enviromental Science, Volume 8, de A. Bytnerowicz, M. Arbaugh, A. Riebau et Andersen C., 79-107. Elseivier BV, 2009.

[34] R.J. Yokelson, I.R. Burling, S.P. Urbanski, E.L. Atlas, K. Adachi, P.R. Buseck, C. Wiedinmyer, S.K. Akagi, D.W. Toohey, C.E. Wold, Trace gas and particle emissions from open biomass burning in Mexico. Atmos. Chem. Phys 11 (2011) 6787-6808.

[35] C.A. Pio, M. Legrand, C.A. Alves, T. Oliviera, J. Afonso, A. Caseiro, H. Puxbaum, A. Sanchez-Ochoa, A. Gelencsér, Chemical composition of atmospheric aerosols during the 2003 summer intense forest fire period. Atmos. Environ. 42 (2008) 7530-7543.

[36] T.G. Soares Neto, J.A.Jr, Carvalho, E.V. Cortez, R.G. Azevedo, R.A. Oliviera, W.R.R. Fidalgo, J.C. Santos, aboratory evaluation of Amazon forest biomass burning emissions. Atmos. Environ. 45 (2011) 7455-7461.

[37] V. Tihay-Felicelli, P.A. Santoni, G. Gerandi, T. Barboni, Smoke emissions due to green waste burning in Mediterranean area: influence of fuel moisture content and fuel mass, Atmos. Environ. 159 (2017) 92–106.

[38] T. Barboni, L. Leonelli, V. Tihay, P.A. Santoni, Influence of the particle size on the heat release rate and the smoke opacity during the burning of dead cistus at laboratory scale, J. Fire Sci. 35 (2017) 259–283

[39] Y. Pérez-Ramirez, W.E. Mell, P.A. Santoni, J.B. Tramoni, F. Bosseur, Examination of WFDS in Modeling Spreading Fires in a Furniture Calorimeter, Fire Tech. 53 (2017) 1795–1832.

[40] N. Frangieh, D. Morvan, S. Meradji, G. Accary, O. Bessonov, Numerical simulation of grassland fires behavior using an implicit physical multiphase model, Fire Safety J. 102 (2018) 33-47.

[41] F. Morandini, P.A. Santoni, J.B. Tramoni, W.E. Mell, Experimental investigation of flammability and numerical study of combustion of shrub of rockrose under severe drought conditions, Fire Safety J. 108 (2019), 102836.

[42] V. Tihay-Felicelli, P.A. Santoni, L. Leonelli, T. Barboni, Autoignition of dead shrub twigs: Influence of diameter on ignition. Fire Thech. 52 (2016) 897–929.

[43] G. Cruz, B.W. Butler, D.X. Viegas, P. Palheiro, Characterization of flame radiosity in shrubland fires. Combust. Flame 158 (2011) 1970–1976.

[44] P.A. Santoni, E. Romagnoli, N. Chiaramonti, T. Barboni, Scale effects on the heat release rate, smoke production rate, and species yields for a vegetation bed. J. Fire Sci. 33 (2015) 290-319.

[45] N. Chiaramonti, E. Romagnoli, P.A. Santoni, T. Barboni, Comparison of the thermal degradation of pine species, utilisation of two sizes of calorimeter: cone calorimeter and LSHR, Fire Technol. 53 (2017) 741–770.

[46] W.A. König, D.H. Hochmuth, D. Joulain, Terpenoids and Related Constituents of Essential Oils.' Library of Massfinder 2.1. University of Hamburg, Institute of Organic Chemistry: Hamburg, 2001.

[47] NIST (National Institute of Standards and Technology). Spectral Database for Organic Compounds, NIST WebBook. Available: http://webbook.nist.gov/chemistry, 2008.

[48] T. Barboni, G. Pellizzaro, B. Arca, N. Chiaramonti, P. Duce, Analysis and origins of volatile organic compounds smoke from ligno-cellulosic fuels. J.Anal. Appl. Pyrol. 89 (2010) 60-65.

[49] L. Leonelli, T. Barboni, P.A. Santoni, Y. Quilichini, A. Coppalle, Characterization of aerosols emissions from the combustion of dead shrub twigs and leaves using a cone calorimeter. Fire Safety J. 91 (2017) 800-810.

[50] S. Hosseini, S.P. Urbanski, P. Dixit, L. Qi, I.R. Burling, R.J. Yokelson, T.J. Johnson, M. Shrivastava, H.S. Jung, E.R. Weise, J.W. Miller, D.R. Cocker, Laboratory characterization of PM emissions from combustion of wildland biomass fuels. J. Geophysical Res. Atmos. 118 (2013) 9914-9929.

[51] J. Aurell, B.K. Gullett, D. Tabor, Emissions from southeastern U.S. Grasslands and pine savannas: Comparison of aerial and ground field measurements with laboratory burns. Atmos. Environ. 111 (2015) 170-178.

[52] E. Romagnoli, T. Barboni, P.A. Santoni, N. Chiaramonti, Quantification of volatile organic compounds in smoke from prescribed burning and comparison with occupational exposure limits. Nat. Hazards and Earth Sys. 14 (2014) 1-9.

[53] C.C. Hardy, S.G. J.C. Conard Regelbrugge, D.R. Teesdale, Smoke emissions from prescribed burning of southern California chaparral. Research paper, Forest Service, Pacific Northwest research station, Portland: United States Department of Agriculture 37, 1996.

[54] E. Garcia-Hurtado, J. Pey, M.J. Baeza, A. Carrara, J. Llovet, X. Querol, A. Alastuey, R. Vallejo, Carbon emissions in Mediterranenan shrubland wildfires: An experimental approach. Atmos. Environ. 69 (2013) 86-93.

[55] R.J. Yokelson, et al., Coupling field and laboratory measurements to estimate the emission factors of identified and unidentified trace gases for prescribed fires. Atmos. Chem. Phys. (2013) 89-116.

946 [56] A. Vicente, C. Alves, A.I. Calvo, A.P. Fernandes, T. Nunes, C. Monteiro, S.M. Almeida,
947 C. Pio, Emission factors and detailed chemical composition of smoke particles from
948 the 2010 wildfire season. Atmos. Environ 71 (2013) 295-303.

949 [57] T. Barboni, L. Leonelli, P.A. Santoni, V. Tihay-Felicelli, Study of the burning of
950 Pteridium aquilinum L. and risk for the personnel involved: Thermal properties and
951 chemical risk, Fire Safety J. 110 (2019) 102904

952

953

954